JACS
JOURNAL OF THE AMERICAN CHEMICAL SOCIETY
Article
pubs.acs.org/JACS

Macyranones: Structure, Biosynthesis, and Binding Mode of an Unprecedented Epoxyketone that Targets the 20S Proteasome

Lena Keller,[†,∥] Alberto Plaza,[†,∥,#] Christian Dubiella,[⊥] Michael Groll,[⊥] Marcel Kaiser,[§,‡] and Rolf Müller*[,†,∥]

[†]Department of Microbial Natural Products, Helmholtz-Institute for Pharmaceutical Research Saarland (HIPS), Helmholtz Centre for Infection Research (HZI) and Pharmaceutical Biotechnology, Saarland University, Campus C2 3, 66123 Saarbrücken, Germany

[∥]German Center for Infection Research (DZIF), Partner site Hannover-Braunschweig 38124, Germany

[§]Swiss Tropical and Public Health Institute (Swiss TPH), Socinstraße 57, CH-4002 Basel, Switzerland

[‡]University of Basel, Petersplatz 1, CH-4003 Basel, Switzerland

[⊥]Center for Integrated Protein Science Munich (CIPSM), Department für Chemie, Technische Universität München, Lichtenbergstraße 4, 85747 Garching, Germany

Supporting Information

ABSTRACT: In our screening efforts to identify unique scaffolds from myxobacteria for the drug discovery process, we used LC-SPE-NMR-MS techniques to isolate six linear peptides, termed macyranone A−F, from *Cystobacter fuscus* MCy9118. The macyranones are characterized by a rare 2-methylmalonamide moiety and an α-amino ketone fragment including an α',β'-epoxyketone in macyranone A. Gene disruption experiments confirmed the biosynthetic gene cluster of the macyranones as PKS/NRPS hybrid. Detailed *in silico* and phylogenetic analysis unraveled that the biosynthesis involves two conspicuous amide bond formations accomplished by an amidotransferase and a unique condensation domain. The gene cluster provides further insights into the formation of the powerful epoxyketone residue involving an acyl-CoA dehydrogenase and an unconventional free-standing thioesterase. Macyranone A was found to inhibit the chymotrypsin-like activity of the yeast 20S proteasome with an IC_{50} of 5.9 nM and the human constitutive proteasome and immunoproteasome with IC_{50} values of 21 and 15 nM, respectively. The β5 subunit of the 20S proteasome was characterized as target by X-ray crystallography revealing an irreversible binding mode similar to the natural product epoxomicin. The presence of the methylmalonamide residue facilitates the stabilization of macyranone A with the active β5 subunit of the proteasome. Macyranone A exhibits a potent inhibitory effect against the parasites *Trypanosoma brucei rhodesiense* and *Leishmania donovani* with IC_{50} values of 1.55 and 0.22 μM, respectively.

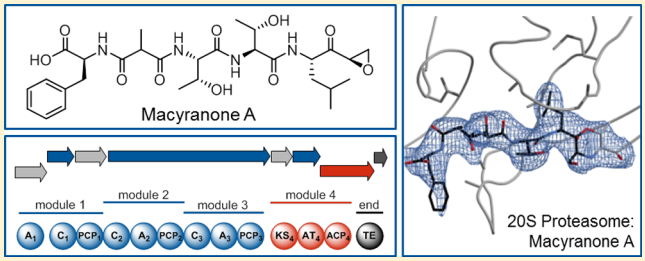

INTRODUCTION

The proteasome aroused the interest as a therapeutic target because of its involvement in many cellular processes like cell cycle control, transcriptional regulation and apoptosis.[1] To date, two proteasome inhibitors have been approved by the FDA for the treatment of blood cancers such as multiple myeloma and mantle cell lymphoma: the peptide boronate bortezomib and the peptidic epoxyketone carfilzomib. Unlike bortezomib, which belongs to the first class of synthetic proteasome inhibitors, carfilzomib directly emerged from the natural product epoxomicin.[2,3] Another promising drug candidate with natural origin is salinosporamide A which was isolated from the marine actinomycete *Salinispora tropica*.[4] Moreover, the evaluation of proteasome-type specific ligands gave rise to alternative strategies to treat chronic inflammation disorders like rheumatoid arthritis and multiple sclerosis[5] as well as infectious diseases including malaria[6] and human sleeping sickness.[7] The common target of all these compounds is the 20S core particle of the proteasome, which is formed by two outer α-rings and two inner β-rings that are composed of seven different α- and seven different β-subunits, respectively. The two β-rings form a barrel-like architecture in which the substrate proteins are cleaved to smaller peptide fragments by the catalytically active subunits β1, β2 and β5.[1] Although these subunits all share an N-terminal threonine (Thr1) as active site nucleophile, β1, β2, and β5 differ in their substrate specificity for cleavage after acidic, basic, and hydrophobic residues, hence being attributed to caspase-like (C-L), trypsin-like (T-L), and chymotrypsin-like (CT-L) activity, respectively.[8,9] Currently, proteasome inhibitors bearing an α',β'-epoxyketone pharmacophore represent the benchmark for specific proteasome blockage by exploiting both nucleophiles, Thr1O$^{\gamma}$ and Thr1N. Their inhibitory mechanism results in the irreversible formation of a morpholine ring, thereby discriminating against other serine-, cysteine-, or aspartate proteases.[10] To date, epoxyke-

Received: February 9, 2015
Published: June 8, 2015

DOI: 10.1021/jacs.5b03833
J. Am. Chem. Soc. 2015, 137, 8121−8130

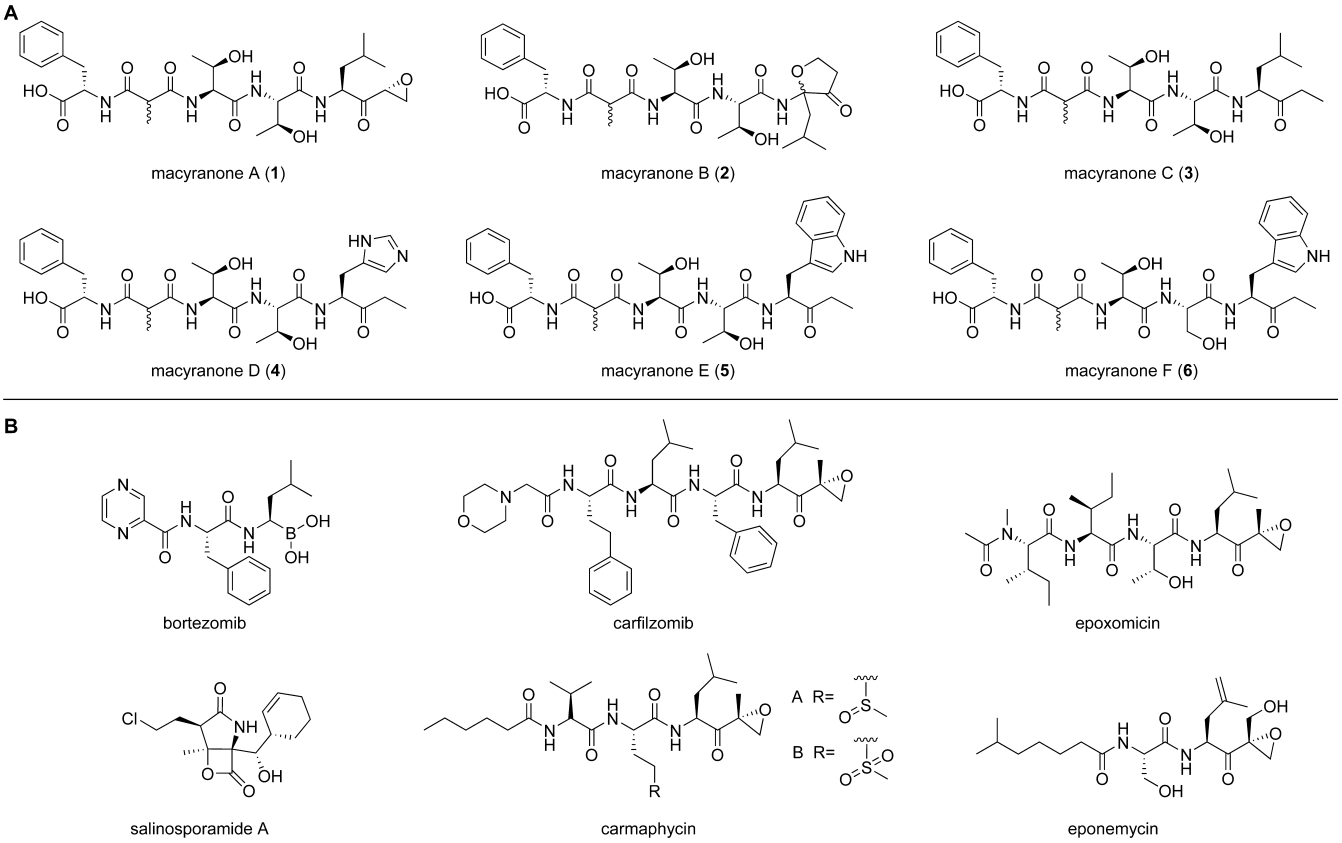

Figure 1. (A) Structures of the macyranones A–F. (B) Structures of verified proteasome inhibitors.

tones have mainly been isolated from actinobacteria[3,11−13] and with the recent discovery of the carmaphycins[14,15] also from cyanobacteria. The biosynthetic gene clusters of the natural peptidyl-epoxyketones eponemycin (Epn) and epoxomicin (Epx) were characterized only recently and gave the first insights into the biosynthesis of the epoxyketone warhead.[16] Recent metagenomic analysis that targets epoxyketone proteasome inhibitors revealed that related gene clusters can be found in a wide range of phylogenetically distinct clades.[17] Herein, we report the isolation of the first epoxyketone proteasome inhibitor from myxobacteria, termed macyranone A (**1**), together with five structural analogues (**2**–**6**). Since the discovery of the first antibiotic myxothiazol[18] from myxobacteria in 1980, they have become well-known for their capability to produce a wide range of secondary metabolites.These gliding bacteria have proven to be a rich source of structurally intriguing and bioactive natural products,[19] many of which originate from mixed polyketide-nonribosomal peptide biosynthetic pathways.[20] Their underlying biosynthetic machineries are termed nonribosomal peptide synthases (NRPSs) and polyketide synthetases (PKSs) and represent large multimodular enzymes in which each module is responsible for the selection, activation, and incorporation of one building block. Such building blocks are usually simple activated short chain dicarboxylic acids such as malonyl-CoA or proteinogenic as well as nonproteinogenic amino acids used to generate a wide range of structurally complex and diverse natural products.

In the search for new natural products from myxobacteria, our focus lies on the identification of new scaffolds in a structure-guided isolation approach. We have been applying LC-SPE-NMR to screen crude extracts for distinct structural elements. Using this approach, we recently isolated a number of new natural products bearing unusual scaffolds including the jahnellamides,[21] the hyalachelins,[22] and the cystomanamides.[23]

RESULTS AND DISCUSSION

In the course of metabolic profiling of *Cystobacter fuscus* MCy9118 using the NMR screening approach based on structural features, an unknown compound family was detected together with the previously reported cystomanamides and the known antibiotics althiomycin, roimatacene, and myxochelin A and B.[23] The small molecules, termed macyranones, were isolated from a large-scale shake flask cultivation of the myxobacterial strain using fractionation via size-exclusion chromatography in combination with reversed-phase HPLC for purification of the compounds. Macyranone A was the most abundant derivative with a yield of 5.2 mg isolated from 10 L cultivation volume.

Structure Elucidation. HRESIMS of macyranone A displayed an ion peak at m/z 607.2987 $[M + H]^+$ (calcd for $C_{29}H_{43}N_4O_{10}$, 607.2974, Δ = 1.97 ppm), consistent with the molecular formula $C_{29}H_{42}N_4O_{10}$ containing 11 double-bond equivalents (DBE). The ^{1}H NMR spectrum of **1** in methanol-d_4 exhibited signals characteristic of a peptide including four α-proton signals at δ 4.68 (1H, dd, J = 9.0, 4.8 Hz), 4.34 (1H, d, J = 4.0 Hz), 4.37 (1H, d, J = 6.2 Hz), and 4.50 (1H, dd, J = 10.4, 4.0 Hz) along with five methyl signals at δ 0.92 (3H, d, J = 6.5 Hz), 0.96 (3H, d, J = 6.6 Hz), 1.16 (3H, d, J = 6.4 Hz), 1.20 (3H, d, J = 6.4 Hz), and 1.26 (3H, d, J = 7.2 Hz) (see Table S1). Additionally, a downfield pair of triplets at δ 7.28 (2H, t, J = 7.5 Hz) and 7.21 (1H, t, J = 7.5 Hz) and a doublet at δ 7.23 (2H, d, J = 7.5 Hz) characteristic of a phenyl group were observed. The HSQC spectrum revealed the presence of two

DOI: 10.1021/jacs.5b03833
J. Am. Chem. Soc. 2015, 137, 8121−8130

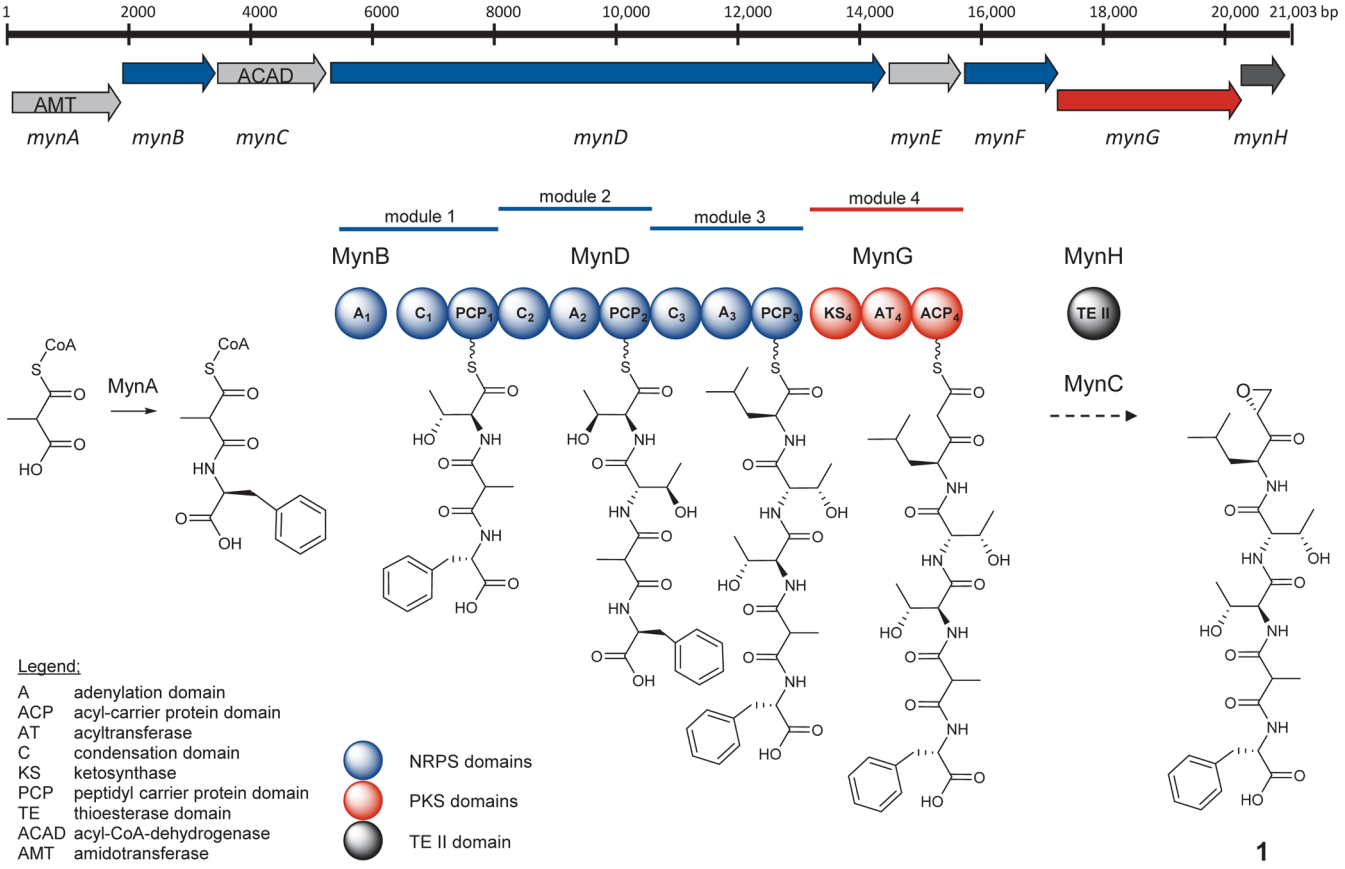

Figure 2. Gene cluster of the macyranones in *Cystobacter fuscus* MCy9118 and the deduced biosynthetic pathway of **1**.

methines ($\delta_{C\text{-}4ekLeu}$ 25.8, $\delta_{H\text{-}4ekLeu}$ 1.72 and $\delta_{C\text{-}1'ekLeu}$ 52.7, $\delta_{H\text{-}1'ekLeu}$ 3.63), two oxygenated methines ($\delta_{C\text{-}3Thr}$ 68.1, $\delta_{H\text{-}3Thr}$ 4.17, $\delta_{C\text{-}3aThr}$ 68.6, $\delta_{H\text{-}aThr}$ 4.04), and three methylene groups ($\delta_{C\text{-}2'ekLeu}$ 47.5, $\delta_{H\text{-}2'ekLeu}$ 3.02/2.98, $\delta_{C\text{-}3ekLeu}$ 39.6, $\delta_{H\text{-}3ekLeu}$ 1.55/1.50 and $\delta_{C\text{-}3Phe}$ 38.2, $\delta_{H\text{-}3Phe}$ 3.26/2.98). A detailed analysis of the 2D NMR data obtained from HSQC, HMBC, and DQF-COSY experiments established the presence of phenylalanine, two threonine residues, a leucine-derived epoxyketone residue (ekLeu), and a 2-methylmalonamide residue (Mma). The latter was identified by a COSY correlation from the methine proton at δ 3.33 (H-2_{Mma}) to methyl protons at δ 1.26 (Me-4_{Mma}) and HMBC correlations from the methine proton at δ 3.33 (H-2_{Mma}) to the two carbon resonances at δ 173.2 (C-1_{Mma} and C-3_{Mma}). The structure of the remaining $C_8H_{14}NO_2$ was deduced as follows. A sequential spin system starting from the α-proton at δ 4.50 (H-2_{ekLeu}) and followed by two methylene protons at δ 1.55/1.50 (H-3_{ekLeu}), the methine proton at δ 1.72 (H-4_{ekLeu}), and two methyl groups at δ 0.92 and 0.96 (Me-5_{ekLeu} and Me-6_{ekLeu}), which are typical signals for a leucine residue, were deduced from TOCSY and COSY spectra. However, an HMBC correlation from H-2_{ekLeu} to the ketone resonance at δ 207.7 was indicative of a modified leucine residue. Indeed, HMBC correlations from H-3_{ekLeu} and the methylene protons at δ 3.02/2.98 (H-$2'_{ekLeu}$) to the ketone resonance as well as from the methine at δ 3.63 (H-$1'_{ekLeu}$) to the α-carbon at δ 54.1 (C-2_{ekLeu}) and a COSY correlation between H-$1'_{ekLeu}$ and H-$2'_{ekLeu}$ clearly identified the presence of a leucine derived α',β'-epoxyketone. The complete sequence was established as Phe-Mma-Thr-aThr-ekLeu through HMBC correlations between α-protons to carbonyl carbons of adjacent residues (Figure S1). In addition, the composition of **1** was supported by ESI-MS/MS measurements. The MS^2 spectrum of the major ion peak at m/z 607 displayed ions at m/z 432 $[M + H\text{-ekLeu-}H_2O]^+$, m/z 331 $[M + H\text{-aThr-ekLeu-}H_2O]^+$, and m/z 230 $[M + H\text{-Thr-aThr-ekLeu-}H_2O]^+$. Thus, the fragmentation patterns were in agreement with the structure of **1** determined by NMR.

An intramolecular rearrangement of the epoxide ring present in macyranone A results in the furanone moiety (fuLeu) that is found in macyranone B (**2**). Besides macyranone A and B, four additional analogues (**3**–**6**) were isolated from the crude extract (Figure 1A).

The molecular formula of macyranone C (**3**) was established to be $C_{29}H_{44}N_4O_9$ (m/z 593.3181 $[M + H]^+$). Its NMR data (Table S2) closely resemble that of **1**, except for the replacement of signal belonging to the epoxide group for an ethyl group (etLeu) ($\delta_{C\text{-}2'etLeu}$ 8.4, $\delta_{H\text{-}2'etLeu}$ 0.99; $\delta_{C\text{-}1'etLeu}$ 33.7, $\delta_{H\text{-}1'etLeu}$ 2.56). Macyranone D and E (**4** and **5**) turned out to be composed of $C_{29}H_{40}N_6O_9$ (m/z 617.2938 $[M + H]^+$) and $C_{34}H_{43}N_5O_9$ (m/z 666.3121 $[M + H]^+$), respectively. The NMR data (Table S2) revealed that their amino acid sequence is identical to that of **3**, only differing by the occurrence of histidine in **4** and tryptophan in **5** instead of leucine. Macyranone F (**6**) displays an ion peak at m/z 652.2933 $[M + H]^+$ (corresponding to a molecular formula $C_{33}H_{41}N_5O_9$) which lacks 14 Da compared to **5**. In fact, a threonine residue is replaced by a serine residue as revealed by NMR data (Table S2).

The absolute configurations of the amino acid residues in the natural products were determined by MS detected chromatographic analysis of the L- and D-FDLA (1-fluoro-2,4-dinitrophenyl-5-L/D-leucinamide) derivatives of the acid hydrolyzate of macyranone A–F (Table S4).[24] It was found that all the

DOI: 10.1021/jacs.5b03833
J. Am. Chem. Soc. 2015, 137, 8121–8130

amino acid residues present in the macyranones possess L-configuration. Moreover, LC-MS analysis indicated the presence of L-threonine and L-*allo*-threonine in compounds **1**−**5**. The absolute configurations of the two threonine residues were determined in **5** by *J*-based configuration analysis.[25] A large coupling constant of $^{3}J_{H-H}$ = 6.5 Hz indicated an anti orientation between H-2$_{aThr}$ and H-3$_{aThr}$. Additionally, a ROESY spectrum recorded in DMSO-d_6 displayed a correlation from NH$_{aThr}$ to Me-4$_{aThr}$ (see Figure S2). Taken together, these data reveal an *erythro* configuration for C-2$_{aThr}$ and C-3$_{aThr}$ thereby establishing the absolute configuration of Thr and aThr as L-threonine and aThr as L-*allo*-threonine. Identical configurations for **1**−**5** were assumed at comparable chiral centers based on the similarities of their structures and NMR data.

The *R* configuration of the epoxyketone warhead was deduced via the co-crystal structure of macyranone A in complex with the 20S proteasome as described for epoxomicin,[10] which is illustrated by the structural superposition in Figure 4. For macyranone B, we observe that the conversion of **1** is not stereospecific since it yields the respective stereocenter as racemic mixture in **2**. Further, the 2-methylmalonamide residue present in all macyranones undergoes a fast proton exchange which leads to a natural racemate at this center.

Identification of the *myn* Biosynthetic Gene Cluster. The chemical structures of the macyranones suggest that the compounds are products of a PKS and NRPS hybrid. The building blocks of the macyranones are expected to include L-phenylalanine, methylmalonyl-CoA, L-threonine, L-*allo*-threonine, or L-serine, a variable amino acid (leucine, histidine or tryptophan), and a malonyl-CoA unit. Using the bioinformatic prediction tool antiSMASH 2.0,[26] a candidate PKS/NRPS biosynthetic gene cluster (*myn*) was identified. The predicted gene cluster consists of eight open reading frames with an overall GC content of 70.0%. Analysis of the catalytic domains led to the prediction of three NRPS modules and one PKS module (Figure 2). The adenylation domain specificity in the three NRPS modules matched the distinct pattern of building blocks for the core amino acid motif Thr-Thr-Leu (Table S6). Genes that did not yield a prediction for PKS or NRPS domains were analyzed via the BLAST algorithm[27] (blastx: DNA query, AA database) against the nonredundant NCBI database (Table 1, Table S5).

Feeding experiments with labeled sodium propionate [1-^{13}C] and sodium acetate [$^{13}C_2$] revealed the incorporation of methylmalonyl-CoA and malonyl-CoA, respectively. Incorporation of leucine-*d*3 confirmed the biosynthetic origin of the ekLeu residue as leucine-derived (Figure S4).

Table 1. Deduced Functions of Open Reading Frames in the Macyranone Biosynthetic Gene Cluster

protein	proposed function
MynA	amidotransferase
MynB	stand-alone A1$_{Thr}$ domain
MynC	acyl-CoA dehydrogenase
MynD	NRPS (C-PCP, C-A2$_{Thr}$-PCP, C-A3$_{Leu}$-PCP)
MynE	transporter
MynF	stand-alone A4$_{His}$ domain
MynG	PKS (KS-AT-ACP)
MynH	thioesterase type II

Intriguingly, the identified building blocks do not exhibit the typical composition reflecting a sequential N- to C-terminal biosynthesis. Based on the arrangement and presence of modules responsible for the incorporation of building blocks, it seems more likely that the assembly line starts with threonine. Subsequent attachment of phenylalanine and methylmalonyl-CoA occur via an alternative route. MynA shows sequence similarity to a family of asparagine synthetases with the closest similarity to PdmN from the pradimicin pathway[28] (41.6% identity), to RubR from the rubromycin pathway (40.3% identity), and to FdmV from the fredericamycin pathway[29] (39.5% identity). Alignment of the three enzymes together with the typical asparagine synthetase B-like amide synthetase (AS B) from *E. coli* (20.5% identity) as shown in Figure S5 suggests that MynA is accountable for amide bond formation between the methylmalonic acid residue and phenylalanine via an AMP intermediate with phenylalanine acting as amino donor. The first adenylation domain found in the identified *myn* biosynthetic gene cluster is a stand-alone adenylation domain with threonine substrate specificity predicted for *mynB*. The coupling of the methylmalonate-phenylalanine and the first threonine could be catalyzed by the condensation domain in the first module of the peptide synthetase as discussed for lipopeptide biosynthesis.[30] Phylogenetic analysis indeed demonstrated a highly unusual nature of this C domain since it does not group with other known types like $^{L}C_L$ type, $^{D}C_L$ type, starter, hybrid, cyclization, epimerization or dual function condensation domains (Figure S6).

Alternatively, the stand-alone adenylation domain encoded by *mynB* is a possible candidate for the amide bond formation as shown for *orf19*, which encodes an amidating stand-alone A domain in streptothricin biosynthesis.[31] Comparison of the adenylation domains did not provide valuable information about the possible function of MynB.

The biosynthesis continues with MynD. Besides the condensation domain and the PCP from the first module, the protein contains two additional modules where the adenylation domains show specificity for threonine and leucine, respectively. These two modules correspond to the sequence of the amino acid residues in the main product macyranone A although no epimerase domain was identified to explain the emergence of L-*allo*-threonine. *MynF* encodes a second stand-alone adenylation domain with histidine substrate specificity (Table S6).

Since some of the macyranones contain a leucine residue (macyranone A−C) and some contain a histidine (D) or tryptophan residue (E and F), MynF might act as an alternative adenylation domain for module 3. The PKS which is responsible for the attachment of the C terminal malonyl-CoA unit is localized on *mynG*. Although active site analysis of the respective AT domain predicted the incorporation of an unusual substrate (Table S7), feeding experiments with sodium acetate [$^{13}C_2$] indicated the incorporation of malonyl-CoA (Figure S4). *MynE* seems to encode a transporter whereas *mynH* encodes a thioesterase type II. The latter protein exhibits some unusual features as revealed by phylogenetic analysis (Figure S8). As a consequence of sequence similarity to a group of thioesterase domains characterized on the basis of the ajudazol TE (AjuTE) by Buntin et al. in 2010,[32] we believe that the type II TE domain present at the terminus of the *myn* gene cluster plays a crucial role in the release of the substrate from the assembly line and therefore in the formation of the epoxyketone unit. In comparison to the biosynthesis of the

DOI: 10.1021/jacs.5b03833
J. Am. Chem. Soc. 2015, 137, 8121−8130

epoxyketones epoxomicin and eponemycin (**12**),[16] only eponemycin biosynthesis involves a similar free-standing TE (EpnB) that also shows 37.5% similarity to MynH on the protein level. In contrast to the *myn* cluster, both clusters contain an integrated type I TE domain downstream of the final PKS module. Comparing the recently identified biosynthetic gene clusters of epoxomicin (*epx*) and eponemycin (*epn*) to the identified cluster of macyranone, it is striking that all three clusters encode an acyl-CoA dehydrogenase (*mynC*, *epxF*, and *epnF*), indicating a major role for this protein in the biosynthesis of the epoxyketone warhead. For epoxomicin and eponemycin, the authors suggested[16] a release of the intermediates as carboxylic acids by the C-terminal thioesterase domain with subsequent reduction and epoxidation accomplished by the acyl-CoA dehydrogenase (ACAD EpxF/EpnF) and a cytochrome P450 (CYP) monooxygenase (EpxC/EpnI), respectively. Alternatively, a mechanism that involves a putative C-methyltransferase domain found in both clusters with subsequent decarboxylation that initiates the epoxide formation by the ACAD and CYP P450 was taken into consideration. However, in contrast to the *epx* and *epn* clusters, the gene cluster of macyranone does not contain a gene that encodes for a CYP P450 enzyme. Even if several CYP P450 homologues were found in the MCy9118 genome, no close relative to EpxC/EpnI was identified. Additionally, no C-methyltransferase domain was identified in the final PKS module (as reasoned by the unsubstituted epoxide ring of **1**) compared to epoxomicin and eponemycin.

Based on our findings, we take another mechanism for epoxyketone formation into consideration: MynC as well as EpxF and EpnF resemble very-long chain acyl-CoA dehydrogenases (VLCAD) isolated from mammalian sources. VLCAD are responsible for α,β-dehydrogenation of long-chain fatty acid acyl-CoA conjugates.[33] Members of the ACAD superfamily belong to the flavoproteins and were shown to catalyze various redox reactions including α,β-dehydrogenation, oxidation of nitroalkanes[34] as well as desulfurization.[35] Acyl-CoA dehydrogenases in general act on CoA esters rather than on free fatty acids.[36] Thus, we suggest as alternative an acyl-carrier-bound mechanism involving the acyl-CoA dehydrogenase MynC. A reductive mechanism similar to such catalyzed by reductase domains[37,38] in combination with simultaneous oxidation of the α-position of the ketone catalyzed by MynC could lead to a release of the compound as an epoxyketone. Chain release may be spontaneous or involve the free-standing thioesterase MynH resulting in the epoxide (**1**) ring formation. Full reduction of the product might lead to macyranone C−F. Obviously, formation of the epoxyketone requires further analysis by biochemical studies. Figure 2 illustrates the genetic organization of the macyranone PKS/NRPS hybrid biosynthetic gene cluster as determined by *in silico* analysis including a biosynthetic hypothesis. Interestingly, *Cystobacter fuscus* DSM2262 (the type strain of the species) contains a very similar gene cluster (95% identity on DNA level) whereas the DNA regions flanking the two clusters are very different and do not contain genes obviously connected to secondary metabolite production. The *C. fuscus* DSM2262 gene cluster might correspond to a gene cluster identified by Schorn et al.[16] where the ACAD from the epoxomicin gene cluster was employed as a probe for a BLAST sequence homology search in the National Center for Biotechnology Information (NCBI) database. Analysis of the chemical profile of *C. fuscus* grown in VY/2S medium showed that also the type strain produces macyranone A, however the production titer is negligible.

Gene Disruption in MCy9118. To confirm that the identified candidate gene cluster is responsible for macyranone production, a single crossover knockout strategy was established. Gene disruption in MCy9118 via single crossover homologous recombination was accomplished according to a previously described protocol.[23]

Therefore, a homologous fragment of each target gene was amplified from genomic DNA using the respective oligonucleotides that additionally inserted stop codons on each side of the fragment. The fragment was ligated into the vector pCRII-TOPO, resulting in the respective pTOPO derivative for gene disruption. The amplified plasmid was introduced into MCy9118 by electroporation. Mutant clones were used to inoculate liquid medium for secondary metabolite analysis and isolation of genomic DNA for genetic verification by PCR. HPLC analysis of the resulting *mynA*, *mynC*, and *mynD* mutants revealed that inactivation of all three genes abolished the production of the macyranones (Figure 3). These results confirm that the identified candidate biosynthetic gene cluster is indeed responsible for macyranone production.

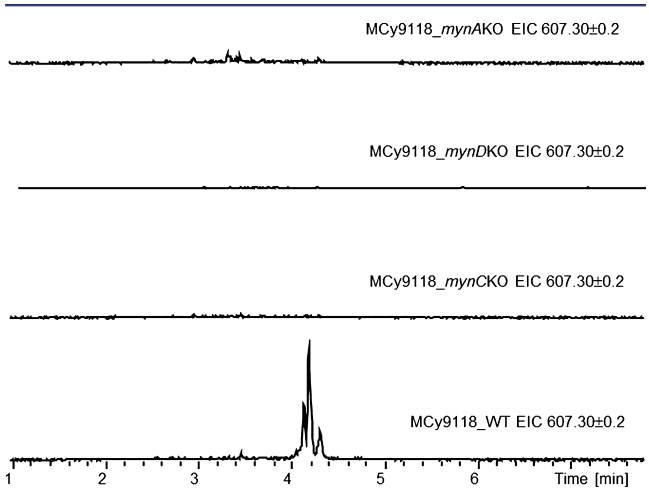

Figure 3. Loss of the macyranone A and B production in the MCy9118 knockout mutants *mynA*KO, *mynD*KO and *mynC*KO as detected by comparative HPLC-MS analysis of MCy9118 wildtype and mutant strains. An extracted ion chromatogram for the $[M + H]^+$ signal of macyranone A and B is shown.

Mode of Action of Macyranone A Toward the 20S Proteasome. Macyranone A inhibits the CT-L activity of the yeast 20S proteasome with an IC_{50} of 5.9 nM. It does not show an effect on the C-L activity whereas it modulates the T-L activity with an IC_{50} of 400 nM. Macyranone B, D, and E did not block any active site up to a tested concentration of 10 μM. Next, **1** was tested against the human constitutive proteasome (cCP) and immunoproteasome (iCP). Both subunits were simultaneously inhibited with an IC_{50} of 21 and 15 nM, respectively. However, surprisingly, macyranone A does not show the expected high cytotoxicity against mammalian cell lines such as the human colon carcinoma HCT-116 cell line, the human leukemia cell lines THP-1 and HL-60, and the rat myoblast cell line L-6. To characterize the binding mode of macyranone A, we determined the crystal structure of the yeast 20S proteasome in complex with macyranone A (2.8 Å resolution, R_{free} = 21.9%, PDB ID 5AHJ). Consistent with the

DOI: 10.1021/jacs.5b03833
J. Am. Chem. Soc. 2015, 137, 8121−8130

proteasome:epoxomicin complex structure, macyranone A binds to the catalytically active Thr1 of subunit β5 as well as β1 and β2, due to the high concentration of the ligand (10 mM) used for crystal soaking experiments (Figure 4).[10] The

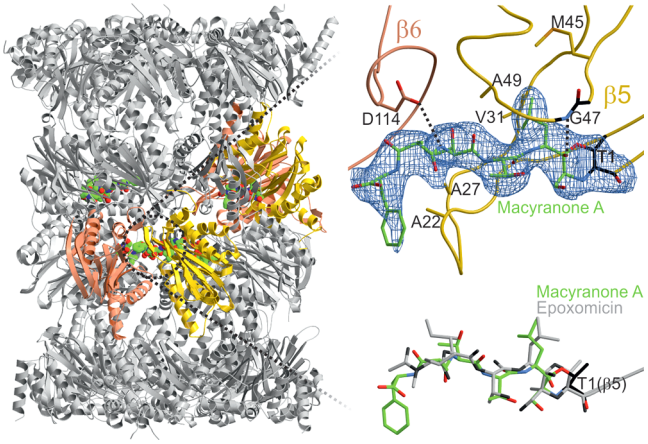

Figure 4. (A) X-ray crystallographic binding analysis of macyranone A bound to the yeast 20S proteasome (PDB ID 5AHJ). (B) The $2F_o-F_c$ electron density map (cyan mesh, contoured at 1σ) shows bound macyranone A (green) at Thr1 (black) and the oxyanion hole formed by G47 (black). Hydrogen bonding of the ligand to subunit β5 (yellow) and subunit β6 (pale orange) is indicated by black dashed lines. (C) Structural superposition of bound macyranone A (green) and epoxomicin (gray) at the Thr1 of subunit β5 of yCP.

mode of action comprises the nucleophilic attack of both nucleophiles present at the active site, Thr1O$^{\gamma}$ and Thr1N, resulting in an irreversible morpholine ring adduct formation. Due to the bivalent binding to the N-terminal Thr1, macyranone A fulfills the requirement to selectively block the small class of N-terminal threonine nucleophile (Ntn) hydrolases, potentially preventing any off-target activity as shown in the case of the clinically relevant carfilzomib.[39]

Furthermore, macyranone A is stabilized by antiparallel β-sheet formation of the peptide backbone in the substrate binding channel combined with distinct stabilization in the substrate specificity pockets. In this regard, the unusual 2-methylmalonamide unit causes a shift at the end of the peptide scaffold, which allows the C-terminal phenylalanine to hydrophobically interact with Ala22 of subunit β5 to achieve further stabilization. The X-ray crystallographic studies complement the results of the NMR spectroscopic analysis supporting the peptide sequence as well as the assigned stereochemistry of macyranone A.

Moreover, macyranone A shows a potent antiparasitic activity against *Trypanosoma brucei rhodesiense*, the causative agent of the African sleeping sickness and against extracellular grown amastigotes of *Leishmania donovani* causing leishmaniasis (Table 2). The activity against *L. donovani* is lost in the intracellular amastigote assay tested up to a concentration of 30 μM.

Macyranone A degrades in buffered aqueous media comparably to epoxomicin (Figure S3). After 4 days, a time period that represents the average duration of the activity assays, around 15% of the starting concentration of macyranone A is retained compared to 42% for epoxomicin. This result shows that the rather low stability is most likely attributed to the epoxyketone moiety itself and does not reduce the importance of this compound class. Instability is reported for

Table 2. Biological Activity of Macyranone A and Epoxomicin

bioactivity assay	macyranone A IC_{50} [μM]	epoxomicin IC_{50} [μM]
constitutive proteasome (human, 10 μg/mL), β5 subunit	0.021	na
immunoproteasome (human, 10 μg/mL), β5 subunit	0.015	na
20S proteasome (yeast, 0.5 nM), β5 subunit	0.0059	0.0005
Trypanosoma brucei rhodesiense	1.55	0.0028[7]
Leishmania donovani	0.22	na
Plasmodium falciparum	41.6	0.0085[6]
HCT-116	29.2	0.0028
THP-1	38.3	0.0116
HL-60	21.9	0.0042
L-6	>100	na

all members of this structural class, and a short systemic half-life is also reported for the FDA approved drug carfilzomib due to peptidase cleavage and epoxide hydrolysis.[40]

CONCLUSIONS

The macyranones represent a new family of natural products isolated from myxobacteria. Their core structure consists of three amino acid residues, an unprecedented 2-methylmalonamide moiety, and an α-amino ketone fragment formed by condensation of an amino acid and an acetate-derived ethyl unit. In particular, macyranone A bears the powerful epoxyketone warhead found in the group of α',β'-epoxyketones.

The biosynthesis of the macyranones deviates widely from the textbook logic of PKS/NRPS hybrids. During macyranone formation, the amidotransferase and the unconventional condensation domain are involved in two conspicuous amide bond formations comprising unprecedented biochemical reactions. Additionally, a acetyl-CoA dehydrogenase homologue and possibly also the type II thioesterase are involved in the formation of the epoxyketone residue representing highly unusual features where *in silico* analysis can currently only provide an idea of the real biosynthetic mechanism. The identification of the biosynthetic gene cluster, detailed *in silico* analysis, and the confirmation of the gene cluster via gene deletion thus set the stage for further detailed biochemical studies.

Moreover, macyranone A shows a potent activity *in vitro* against the β5 subunit of the human constitutive proteasome as well as the immunoproteasome. X-ray analysis of macyranone A in complex with the yeast 20S proteasome confirms the covalent binding mechanism of the epoxyketones. Furthermore, the unusual 2-methylmalonamide residue was identified to further stabilize the ligand in the substrate binding channel allowing a hydrophobic interaction between the C-terminal phenylalanine and subunit β5.

In closing, these results contribute to our understanding of the selective blockage of the ubiquitous eukaryotic 20S proteasome and could be of help to the development of selective inhibitors. Also, the identification of the biosynthetic gene cluster, detailed *in silico* analysis, and confirmation of the gene cluster via gene deletion set the stage for further studies in the formation of the epoxyketone functionality. Finally, the identification of the epoxyketone proteasome inhibitor macyranone A from myxobacteria provides another example

DOI: 10.1021/jacs.5b03833
J. Am. Chem. Soc. 2015, 137, 8121−8130

of the importance of these gliding bacteria in drug discovery programs.

EXPERIMENTAL SECTION

General Experimental Procedures. NMR spectra were recorded in methanol-d_4 on a Bruker Ascend 700 spectrometer with a 5 mm TXI cryoprobe (^{1}H at 700 MHz, ^{13}C at 175 MHz) or a Bruker Avance III 500 spectrometer with a 5 mm TXI cryoprobe (^{1}H at 500 MHz, ^{13}C at 125 MHz). DQFCOSY, HOHAHA, HSQC, HMBC, and ROESY experiments were recorded using standard pulse programs. HSQC experiments were optimized for $^1J_{C-H}$ = 145 Hz, and HMBC spectra were optimized for $^{2,3}J_{C-H}$ = 6 Hz. The samples were dissolved in methanol-d_4, and the chemical shifts of the solvent signals at 3.31 ppm (δ_H) and 49.15 ppm (δ_C) were considered as internal standard (reference signal). The observed chemical shift (δ) values were given in ppm and the coupling constants (J) in Hz. 5 mm Shigemi tubes (Shigemi Inc., Allison Park, PA 15101, USA) were used to increase sensitivity. A Dionex Ultimate 3000 RSLC system was used for LC-HRMS measurements with a Waters BEHC18, 100 × 2.1 mm, 1.7 μm dp column. Separation of 2 μL sample was achieved by a linear gradient with (A) H_2O + 0.1% FA to (B) ACN + 0.1% FA at a flow rate of 600 μL/min and 45 °C. The gradient was initiated by a 0.5 min isocratic step at 5% B, followed by an increase to 95% B in 18 min to end up with a 2 min step at 95% B before reequilibration with initial conditions. UV spectra were recorded by a DAD in the range from 200 to 600 nm. The LC flow was split to 75 μL/min before entering the maXis HR-ToF mass spectrometer (Bruker Daltonics, Bremen, Germany) using the standard ESI source. Mass spectra were acquired in centroid mode ranging from 150 to 2000 m/z at 2 Hz scan speed.

Cultivation of Strain MCy9118. The myxobacterial strain *C. fuscus* MCy9118 was isolated and cultivated using previously reported methods.[23] For the production of the macyranones, the preculture was used to inoculate 300 mL shake flasks containing a 50 mL VY/2S-DY medium (0.4% dry yeast, 0.05% $CaCl_2 \times 2\ H_2O$, 1.0% soluble starch, 5 mM HEPES adjusted to pH 7.0 with 10 N KOH) that was incubated at 30 °C for 8 h. 20 mL of the cultures were always used to inoculate six times 2 L VY/2S-DY medium containing 8 mg/mL Fe-EDTA in 5 L shake flasks (shaking rate 160 rpm; 30 °C). Two % XAD adsorber resin (Amberlite XAD-7, Sigma) was added to the shake flasks on day 2 of the cultivation. The cultures were incubated for 7 days. Cultures were harvested by sieving the culture to receive the XAD.

Isolation Procedure. XAD was washed with *dd*H_2O to remove salts prior to freeze-drying. The XAD was extracted exhaustively with MeOH to obtain the crude extract. Sephadex fractionation was performed using a GE Healthcare SR 25/100 column, sephadex LH 20 was used for separation, and methanol as the mobile phase. The fractions containing the respective peptides were combined, and the solvent was evaporated. The compounds were separated by preparative HPLC. A Waters Xbridge C18, 150 × 19 mm, 5 μm dp column was used and a linear gradient from 5 to 95% B in 30 min with (A) H2O + 0.1% FA and (B) MeOH + 0.1% FA at a flow rate of 25 mL/min at room temperature. Each injection consisted of up to 150 mg of the combined fractions dissolved in 500 μL MeOH. Fractions were collected by time in test tubes. The compounds were repurified by semipreparative HPLC at 30 °C eluting with a linear gradient and column according to the compound description and a DAD at 220 nm.

Macyranone A (1). ^{1}H and ^{13}C NMR data, see Table S1; HRESIMS m/z 607.2967 $[M + H]^+$ corresponding to a molecular formula $C_{29}H_{42}N_4O_{10}$ (calcd for $C_{29}H_{43}N_4O_{10}$, 607.2974, Δ = 1.2 ppm) Isolation: Phenomenex Synergi 4 μm Fusion-RP 80 Å, LC Column 250 × 10 mm; t_R = 39.5 min; flow rate = 2.5 mL/min; 0−1 min 10% B, 1−45 min 10−90% B; A: H_2O + 0.1% FA, B: MeOH + 0.1% FA.

Macyranone B (2). ^{1}H and ^{13}C NMR data, see Table S2; HRESIMS m/z 607.2963 $[M + H]^+$ corresponding to a molecular formula $C_{29}H_{42}N_4O_{10}$ (calcd for $C_{29}H_{43}N_4O_{10}$, 607.2974, Δ = 1.8 ppm) Isolation: Jupiter 4 μm Proteo 90 Å, LC Column 250 × 10 mm; t_R = 43.9 min; flow rate = 2.5 mL/min; 0−7 min 34% B, 7−47 min 34−75% B; A: H_2O + 0.1% FA, B: MeOH + 0.1% FA.

Macyranone C (3). ^{1}H and ^{13}C NMR data, see Table S2; HRESIMS m/z 593.3181 $[M + H]^+$ corresponding to a molecular formula $C_{29}H_{44}N_4O_9$ (calcd for $C_{29}H_{45}N_4O_9$, 593.3181, Δ = 0 ppm) Isolation: Jupiter 4 μm Proteo 90 Å, LC Column 250 × 10 mm; t_R = 25.1 min; flow rate = 2.5 mL/min; 0−1 min 10% B, 1−45 min 10−90% B; A: H_2O + 0.1% FA, B: ACN + 0.1% FA.

Macyranone D (4). ^{1}H and ^{13}C NMR data, see Table S2; HRESIMS m/z 617.2938 $[M + H]^+$ corresponding to a molecular formula $C_{29}H_{40}N_6O_9$ (calcd for $C_{29}H_{41}N_6O_9$, 617.2930, Δ = 1.3 ppm) Isolation: Synergi 4 μm Polar-RP 80 Å, LC Column 250 × 10 mm; t_R = 23.3 min; flow rate = 3.5 mL/min; 0−1 min 10% B, 1−41 min 10−90% B; A: H_2O + 0.1% FA, B: MeOH + 0.1% FA.

Macyranone E (5). ^{1}H and ^{13}C NMR data, see Tables S2 and S3; HRESIMS m/z 666.3121 $[M + H]^+$ corresponding to a molecular formula $C_{34}H_{43}N_5O_9$ (calcd for $C_{34}H_{44}N_5O_9$, 666.3134, Δ = 2.1 ppm) Isolation: Jupiter 4 μm Proteo 90 Å, LC Column 250 × 10 mm; t_R = 40.7 min; flow rate = 2.5 mL/min; 0−1 min 10% B, 1−45 min 10−90% B; A: H_2O + 0.1% FA, B:ACN + 0.1% FA.

Macyranone F (6). ^{1}H and ^{13}C NMR data, see Table S2; HRESIMS m/z 652.2933 $[M + H]^+$ corresponding to a molecular formula $C_{33}H_{41}N_5O_9$ (calcd for $C_{33}H_{42}N_5O_9$, 652.2977, Δ = 6.7 ppm) Isolation: Jupiter 4 μm Proteo 90 Å, LC Column 250 × 10 mm; t_R = 39.6 min; flow rate = 2.5 mL/min; 0−1 min 10% B, 1−45 min 10−90% B; A: H_2O + 0.1% FA, B: ACN + 0.1% FA.

Advanced Marfey's Method.[41] Approximately 0.2 mg of the compound was hydrolyzed with 6 N HCl (0.8 mL) and shaken at 90 °C for 16 h in Eppendorf tubes. Samples were dried under vacuum and dissolved in H_2O (100 μL). They were split into two 50 μL aliquots, and 1 N $NaHCO_3$ (20 μL) and 1% 1-fluoro-2,4-dinitrophenyl-5-leucine-amide (L-FDLA or D-FDLA solution in acetone, 100 μL) were added, respectively. The mixtures were heated to 40 °C for 40 min and cooled down to RT, and the reaction was quenched by addition of 2 N HCl (20 μL). Solvents were evaporated under nitrogen, and residues were redissolved in 1 mL CH_3CN and subsequently analyzed by LCMS. All measurements were performed on a Dionex Ultimate 3000 RSLC system using a Waters BEH C18, 100 × 2.1 mm, 1.7 μm column by injection of 1 μL sample. Separation was achieved by a gradient using (A) H2O + 0.1% FA to (B) ACN + 0.1% FA at a flow rate of 550 μL/min and 45 °C. The gradient was as follows: starting at 5% B to increase to 10% B in 1 min, from 1 to 15 min increase to 35% B, from 15 to 22 S5 min increase to 50% B, and from 22 to 25 min increase to 80% B. After a 1 min hold at 80% B the system was re-equilibrated with initial conditions for 5 min. UV data were acquired at 340 nm, and MS detection was performed simultaneously. Coupling the HPLC to the MS was supported by an Advion Triversa Nanomate nanoESI system attached to a Thermo Fisher Orbitrap. LC flow is split to 500 nL/min before entering the ion source. Mass spectra were acquired in centroid mode ranging from 150 to 1000 m/z at a resolution of R = 30000. Results can be found in Table S4.

Sequence Analysis. Routine DNA *in silico* sequence analysis was carried out using the Geneious 6.1.6 software. Annotation of the catalytic domains and characterization of the A domain substrate specificity was performed using the tools antiSMASH 2.0,[26] Pfam,[42] NRPSpredictor2,[43] PKS/NRPS Analysis,[44] and NaPDoS.[45]

General Procedures for DNA Manipulation and PCR. Chromosomal DNA from MCy9118 was prepared using the Puregene Core Kit A (Qiagen) according to the manufacturer's instructions. PCR was carried out using Phusion High Fidelity DNA Polymerase (Thermo Scientific) according to the manufacturer's protocol with addition of 5% DMSO to the reaction mixture. For the amplification, conditions were: Initial denaturation step at 98 °C for 2 min, denaturation for 10 s at 98 °C, annealing for 15 s at 60 to 70 °C according to the primer, extension at 72 °C for 2 min (30 cycles), and a final extension step at 72 °C for 10 min. PCR products were purified via agarose gel electrophoresis and subsequent extraction from the gel using the peqGOLD Gel Extraction Kit (Peqlab). Ligation of DNA fragments with sticky ends was done using T4 DNA Ligase (Thermo Scientific) according to the manufacturer protocol using a 4:1 molar

DOI: 10.1021/jacs.5b03833
J. Am. Chem. Soc. 2015, 137, 8121−8130

ratio of insert and vector. Restriction digest was done using enzymes from Thermo Scientific according to the manufacturer's protocol and recommendations regarding double digest. For pTOPO cloning, the TOPO TA Cloning Kit with pCR 2.1 TOPO vector (Invitrogen) was used. Plasmids were introduced into chemically competent *E. coli* strains via heat shock transformation and into *C. fuscus* MCy9118 via electroporation at 650 V and 400 Ω. *E. coli* clones containing a plasmid were selected on LB agar (1.5% agar) supplemented with 50 mg/L Kanamycin-sulfate (Kan) at 37 °C. Mutant clones of MCy9118 were selected on M-agar (1.5% agar) containing 50 mg/L Kan.

Single Crossover Homologous Recombination Strategy. Gene disruption in MCy9118 via single crossover homologous recombination was accomplished according to a previously described protocol.[23] A homologous fragment of each target gene with a size around 1 kb was amplified from genomic DNA using the respective oligonucleotides listed in Table S8 that additionally inserted stop codons on each side of the fragment. The fragment was ligated into the vector pCRII-TOPO, resulting in the respective pTOPO derivative for gene disruption. The plasmids were transformed into *E. coli* strain SCS110 for amplification of the plasmid without Dam or Dcm methylation. The plasmid was recovered from the strain by the alkaline lysis method, and after restriction analysis it was introduced into MCy9118 by electroporation. Single clones were used to inoculate liquid medium (M medium + 50 mg/L Kan) for secondary metabolite analysis and isolation of genomic DNA for genetic verification by PCR. Subsequent HPLC analysis of the resulting *mynA*, *mynC* and *mynD* mutants revealed that inactivation of the three genes abolished production of the macyranones.

To genetically verify the mutants, two PCR reactions were performed for each mutant (see Figure S9). The first PCR was performed with primers that bind outside of the region of plasmid insertion. A product is only generated if the gene is not disrupted by the plasmid backbone so that the mutants should not show a product in contrast to the compared wild type. The second PCR was performed with one primer that binds outside of the region of plasmid insertion and one that binds the plasmid backbone. A product is only generated if the plasmid was inserted in the right position so that the mutants should show a product in contrast to the compared wild type were no product is expected. Mutants fulfilling both conditions were considered as genetically verified.

Activity against *Trypanosoma brucei rhodesiense* STIB900. This stock was isolated in 1982 from a human patient in Tanzania and after several mouse passages cloned and adapted to axenic culture conditions.[46] Minimum essential medium (50 μL) supplemented with 25 mM HEPES, 1 g/L additional glucose, 1% MEM nonessential amino acids (100×), 0.2 mM 2-mercaptoethanol, 1 mM Na-pyruvate, and 15% heat inactivated horse serum were added to each well of a 96-well microtiter plate. Serial drug dilutions of 11 3-fold dilution steps covering a range from 100 to 0.002 μg/mL were prepared. Then 4×10^3 bloodstream forms of *T. b. rhodesiense* STIB 900 in 50 μL was added to each well, and the plate incubated at 37 °C under a 5% CO_2 atmosphere for 70 h. 10 μL Alamar Blue (resazurin, 12.5 mg in 100 mL double-distilled water) was then added to each well and incubation continued for 2−4 h longer.[47] Then the plates were read with a Spectramax Gemini XS microplate fluorometer (Molecular Devices Cooperation, Sunnyvale, CA, USA) using an excitation wavelength of 536 nm and an emission wavelength of 588 nm. The IC_{50} values were calculated by linear regression[48] from the sigmoidal dose inhibition curves using SoftmaxPro software (Molecular Devices Cooperation, Sunnyvale, CA, USA). Melarsoprol (Arsobal Sanofi-Aventis, received from WHO) is used as control.

Activity against *L. donovani* Axenic Amastigotes. Amastigotes of *L. donovani* strain MHOM/ET/67/L82 were grown in axenic culture at 37 °C in SM medium[49] at pH 5.4 supplemented with 10% heat-inactivated fetal bovine serum under an atmosphere of 5% CO_2 in air. 100 μL of culture medium with 10^5 amastigotes from axenic culture with or without a serial drug dilution was seeded in 96-well microtiter plates. Serial drug dilutions of 11 3-fold dilution steps covering a range from 90 to 0.002 μg/mL were prepared. After 70 h of incubation the plates were inspected under an inverted microscope to ensure growth of the controls and sterile conditions. 10 μL of Alamar Blue (12.5 mg resazurin dissolved in 100 mL distilled water)[50] was then added to each well, and the plates incubated for another 2 h. Then the plates were read with a Spectramax Gemini XS microplate fluorometer (Molecular Devices Cooperation, Sunnyvale, CA, USA) using an excitation wavelength of 536 nm and an emission wavelength of 588 nm. Data were analyzed using the software Softmax Pro (Molecular Devices Cooperation, Sunnyvale, CA, USA). Decrease of fluorescence (= inhibition) was expressed as percentage of the fluorescence of control cultures and plotted against the drug concentrations. From the sigmoidal inhibition curves the IC_{50} values were calculated.

Activity against *L. donovani* Intracellular Amastigotes. Macrophage assay:[51] Mouse peritoneal macrophages (4×10^4 in 100 μL RPMI 1640 medium with 10% heat-inactivated FBS) were seeded into wells of Lab-tek 16-chamber slides. After 24 h 1.2×10^5 amastigote *L. donovani* in 100 μL was added. The amastigotes were taken from an axenic amastigote culture grown at pH 5.4. Four hrs later the medium containing free amastigote forms was removed and replaced by fresh medium. The next day the medium was replaced by medium containing different compound dilutions. Parasite growth in the presence of the drug was compared to control wells. After 96 h of incubation the medium was removed, and the slides fixed with methanol for 10 min followed by a staining with a 10% Giemsa solution. Infected and noninfected macrophages were counted for the control cultures and the ones exposed to the serial drug dilutions. The infection rates were determined. The results were expressed as % reduction in parasite burden compared to control wells, and the IC_{50} calculated by linear regression analysis.

Activity against *P. falciparum*. In vitro activity against erythrocytic stages of *P. falciparum* was determined using a ^{3}H-hypoxanthine incorporation assay,[52,53] using the drug sensitive NF54 strain[54] and the standard drug chloroquine (Sigma C6628). Compounds were dissolved in DMSO at 10 mg/mL and added to parasite cultures incubated in RPMI 1640 medium without hypoxanthine, supplemented with HEPES (5.94 g/L), $NaHCO_3$ (2.1 g/L), neomycin (100 U/mL), and Albumax (5 g/L) and washed human red cells A^+ at 2.5% hematocrit (0.3% parasitaemia). Serial drug dilutions of 11 3-fold dilution steps covering a range from 100 to 0.002 μg/mL were prepared. The 96-well plates were incubated in a humidified atmosphere at 37 °C; 4% CO_2, 3% O_2, 93% N_2. After 48 h 50 μL of ^{3}H-hypoxanthine (= 0.5 μCi) was added to each well of the plate. The plates were incubated for a further 24 h under the same conditions. The plates were then harvested with a Betaplate cell harvester (Wallac, Zurich, Switzerland), and the red blood cells transferred onto a glass fiber filter then washed with distilled water. The dried filters were inserted into a plastic foil with 10 mL of scintillation fluid and counted in a Betaplate liquid scintillation counter (Wallac, Zurich, Switzerland). IC_{50} values were calculated from sigmoidal inhibition curves by linear regression[48] using Microsoft Excel. Chloroquine and artemisinin are used as controls.

Cytotoxicity Assay with L-6 cells. Assays were performed in 96-well microtiter plates, each well containing 100 μL of RPMI 1640 medium supplemented with 1% L-glutamine (200 mM) and 10% fetal bovine serum, and 4000 L-6 cells (a primary cell line derived from rat skeletal myoblasts).[55,56] Serial drug dilutions of 11 3-fold dilution steps covering a range from 100 to 0.002 μg/mL were prepared. After 70 h of incubation the plates were inspected under an inverted microscope to ensure growth of the controls and sterile conditions. 10 μL of Alamar Blue was then added to each well, and the plates incubated for another 2 h. Then the plates were read with a Spectramax Gemini XS microplate fluorometer (Molecular Devices Cooperation, Sunnyvale, CA, USA) using an excitation wavelength of 536 nm and an emission wavelength of 588 nm. The IC_{50} values were calculated by linear regression[48] from the sigmoidal dose inhibition curves using SoftmaxPro software (Molecular Devices Cooperation, Sunnyvale, CA, USA). Podophyllotoxin (Sigma P4405) is used as a control.

Cytotoxicity Assay with HCT-116 cells. Growth inhibition experiments (MTT): Cells were seeded at 6×10^3 cells per well of 96-well plates (Corning CellBind) in complete medium (180 μL) and

DOI: 10.1021/jacs.5b03833
J. Am. Chem. Soc. 2015, 137, 8121−8130

directly treated with macyranones dissolved in DMSO in a serial dilution. Each compound was tested in duplicate for 5 d as well as the internal solvent control. After 5 d incubation, 5 mg mL^{-1} MTT in PBS (20 μL) was added per well and was further incubated for 2 h at 37 °C.[57] The medium was then discarded, and cells were washed with PBS (100 μL) before adding 2-propanol/10n HCl (250:1, v/v; 100 μL) in order to dissolve formazan granules. The absorbance at 570 nm was measured using a microplate reader (Infinite M200PRO, Tecan), and cell viability was expressed as a percentage relative to the respective DMSO control. IC_{50} values were obtained by sigmoidal curve fitting.

Cytotoxicity Assay with THP-1/HL-60 cells. Growth inhibition experiments (resazurin): Cells were prepared and treated as described above and seeded in RPMI-1640 medium either containing 0.5 or 10% FBS or 10% of heat-inactivated serum (45 min, 60 °C). After 4 d incubation, 0.5 mg mL^{-1} resazurin in PBS (9 μL) was added per well and was further incubated for 3 h at 37 °C. The viability of cells (resorufin) relative to the solvent control was determined by fluorescence intensity measurement at 590 nm with an excitation wavelength of 540 nm (Infinite M200PRO, Tecan). IC_{50} values were obtained by sigmoidal curve fitting.

Inhibition Assay with 20S Proteasome from Yeast. Compounds were assayed for inhibition of the 20S proteasome as previously described,[58] but using 0.5 nM of 20S proteasome from *Saccharomyces cerevisiae* (Enzo Life Sciences).

Crystallization and Structure Elucidation. yCP crystals were grown in hanging drop plates at 20 °C as previously described,[8,59] using a protein concentration of 40 mg/mL in Tris/HCl (20 mm, pH 7.5) and EDTA (1 mm). The drops contained 1 μL of the reservoir solution consisting of 30 mm $MgAc_2$, 100 mm morpholino-ethanesulfonic acid (MES) (pH 7.2) and 10% (v/v) 2-methyl-2,4-pentanediol as well as 1 μL of protein. Crystals appeared after 48 h and were then soaked with macyranone A in DMSO at final concentrations of 10 mm for 12 h following complementation of the droplets with cryoprotecting buffer consisting of 30% (w/v) 2-methyl-2,4-pentanediol, 20 mm $MgAc_2$, and 100 mm MES (pH 6.9). The crystals were supercooled in a stream of liquid nitrogen gas at 100 K (Oxford Cryo Systems). The data set of yCP:macyranone A structure was collected with 2.8 Å resolution using synchrotron radiation (λ = 1.0 Å) at the X06SA-beamline (Swiss Light Source, Villingen, Switzerland, Table S9). X-ray intensities were assessed with the program XDS,[60] and data reduction was carried out using XSCALE.[60] The molecular replacement started with the coordinates of yCP (pdb entry code: 1RYP), and translation/libration/screw (TLS) refinements were performed with REFMAC5 in the CCP4i suite.[61] Model building was carried out using the program package MAIN.[62]

Proteasome Purification. 20S proteasome from *S. cerevisiae* (yCP) was purified as previously described.[8] The yeast cells were lysed in a continuous cell disruption system and centrifuged at 40,000 *g*. The suspension was applied to a phenyl sepharose HIC column after precipitation in aqueous 40% $(NH_4)_2SO_4$. Eluted fractions with 20S proteasome activity were pooled and purified using a FPLC system with hydroxyapatite column. The polishing was performed via a Resource-Q anion exchange column and Superose 6 size exclusion chromatography. Pooled fractions were concentrated to 40 mg/mL in 20 mm Tris (pH 7.5) and used for vitro assays and crystallization trials.

IC_{50} Value Determination. The *in vitro* proteasome inhibition assays were performed with fluorescence assays in 96-well plates. The assay mixtures contained 10 μg/mL of commercially available purified human cCP (Boston Biochem) and human iCP (Boston Biochem) in 100 mm Tris/HCl (pH 7.5) buffer. Inhibitors were dissolved in DMSO and added at various concentrations with three repetitions each, with a final concentration of <10% (w/v) DMSO. After the incubation time of 60 min at RT, the fluorogenic substrate Suc-Leu-Leu-Val-Tyr-AMC (Bachem) was added to measure the residual activity of the chymotrypsin-like site. Afterward, the assay mixture was incubated for another hour at RT, and fluorescence was determined on a Varian Cary Eclipse photofluorometer with excitation and emission wavelengths of λ_{exc} = 360 and λ_{em} = 460 nm, respectively.

■ ASSOCIATED CONTENT

Supporting Information

Figures and tables giving configuration analysis, inactivation of the *myn* cluster in MCy9118 as well as experimental details, phylogenetic analysis, crystallographic data collection and refinement statistics, NMR assignments, and 1D and 2D NMR spectra for **1**−**6**. The Supporting Information is available free of charge on the ACS Publications website at DOI: 10.1021/jacs.5b03833.

■ AUTHOR INFORMATION

Corresponding Author

*rolf.mueller@helmholtz-hzi.de

Present Address

[#]Fraunhofer IME, Sanofi-Fraunhofer Natural Products Center of Excellence, Industriepark Höchst, Bldg. G878, 65926 Frankfurt/Main, Germany.

Notes

The authors declare no competing financial interest.

■ ACKNOWLEDGMENTS

Research in R.M.'s laboratory was funded by the Bundesministerium für Bildung and Forschung. We thank Dr. Sascha Baumann for assistance with the genetic manipulation of the strain and also Dr. Jennifer Herrmann and Viktoria Schmitt for performing bioactivity assays (all from R.M.'s laboratory). We thank the staff of the beamline X06SA at the Paul Scherrer Institute, Swiss Light Source, Villigen (Switzerland) for assistance during data collection. We are grateful to R. Feicht for large-scale purification of yeast 20S proteasomes.

■ REFERENCES

(1) Huber, E. M.; Groll, M. *Angew. Chem., Int. Ed.* **2012**, *51*, 8708−8720.

(2) Myung, J.; Kim, K. B.; Lindsten, K.; Dantuma, N. P.; Crews, C. M. *Mol. Cell* **2001**, *7*, 411−20.

(3) Hanada, M.; Sugawara, K.; Kaneta, K.; Toda, S.; Nishiyama, Y.; Tomita, K.; Yamamoto, H.; Konishi, M.; Oki, T. *J. Antibiot.* **1992**, *45*, 1746−52.

(4) Fenical, W.; Jensen, P. R.; Palladino, M. A.; Lam, K. S.; Lloyd, G. K.; Potts, B. C. *Bioorg. Med. Chem.* **2009**, *17*, 2175−2180.

(5) Moore, B. S.; Eustáquio, A. S.; McGlinchey, R. P. *Curr. Opin. Chem. Biol.* **2008**, *12*, 434−40.

(6) Kreidenweiss, A.; Kremsner, P. G.; Mordmüller, B. *Malar. J.* **2008**, *7*, 187.

(7) Glenn, R. J.; Pemberton, A. J.; Royle, H. J.; Spackman, R. W.; Smith, E.; Jennifer Rivett, A.; Steverding, D. *Int. J. Antimicrob. Agents* **2004**, *24*, 286−9.

(8) Groll, M.; Ditzel, L.; Löwe, J.; Stock, D.; Bochtler, M.; Bartunik, H. D.; Huber, R. *Nature* **1997**, *386*, 463−471.

(9) Huber, E. M.; Basler, M.; Schwab, R.; Heinemeyer, W.; Kirk, C. J.; Groettrup, M.; Groll, M. *Cell* **2012**, *148*, 727−738.

(10) Groll, M.; Kim, K. B.; Kairies, N.; Huber, R.; Crews, C. M. *J. Am. Chem. Soc.* **2000**, *122*, 1237−1238.

(11) Sugawara, K.; Hatori, M.; Nishiyama, Y.; Tomita, K.; Kamei, H.; Konishi, M.; Oki, T. *J. Antibiot.* **1990**, *43*, 8−18.

(12) Koguchi, Y.; Nishio, M.; Suzuki, S.; Takahashi, K.; Ohnuki, T.; Komatsubara, S. *J. Antibiot.* **2000**, *53*, 967−972.

(13) Koguchi, Y.; Kohno, J.; Suzuki, S.; Nishio, M.; Takahashi, K.; Ohnuki, T.; Komatsubara, S. *J. Antibiot.* **1999**, *52*, 1069−76.

(14) Pereira, A. R.; Kale, A. J.; Fenley, A. T.; Byrum, T.; Debonsi, H. M.; Gilson, M. K.; Valeriote, F. a; Moore, B. S.; Gerwick, W. H. *ChemBioChem* **2012**, *13*, 810−7.

DOI: 10.1021/jacs.5b03833
J. Am. Chem. Soc. 2015, 137, 8121−8130

(15) Trivella, D. B. B.; Pereira, A. R.; Stein, M. L.; Kasai, Y.; Byrum, T.; Valeriote, F. A.; Tantillo, D. J.; Groll, M.; Gerwick, W. H.; Moore, B. S. *Chem. Biol.* **2014**, *21*, 782−91.
(16) Schorn, M.; Zettler, J.; Noel, J. P.; Dorrestein, P. C.; Moore, B. S.; Kaysser, L. *ACS Chem. Biol.* **2014**, *9*, 301−9.
(17) Owen, J. G.; Charlop-Powers, Z.; Smith, A. G.; Ternei, M. a.; Calle, P. Y.; Reddy, B. V. B.; Montiel, D.; Brady, S. F. *Proc. Natl. Acad. Sci. U. S. A.* **2015**, 201501124.
(18) Gerth, K.; Irschik, H.; Reichenbach, H.; Trowitzsch, W. *J. Antibiot.* **1980**, *33*, 1474−1479.
(19) Wenzel, S. C.; Müller, R. *Curr. Opin. Drug Discovery Dev.* **2009**, *12*, 220−30.
(20) Bode, H. B.; Müller, R. *J. Ind. Microbiol. Biotechnol.* **2006**, *33*, 577−88.
(21) Plaza, A.; Viehrig, K.; Garcia, R.; Müller, R. *Org. Lett.* **2013**, *15*, 5882−5.
(22) Nadmid, S.; Plaza, A.; Lauro, G.; Garcia, R.; Bifulco, G.; Müller, R. *Org. Lett.* **2014**, *16*, 4130−3.
(23) Etzbach, L.; Plaza, A.; Garcia, R.; Baumann, S.; Müller, R. *Org. Lett.* **2014**, *16*, 2414−7.
(24) Harada, K.; Fujii, K.; Mayumi, T.; Hibino, Y.; Suzuki, M.; Ikai, Y.; Oka, H. *Tetrahedron Lett.* **1995**, *36*, 1515−1518.
(25) Matsumori, N.; Kaneno, D.; Murata, M.; Nakamura, H.; Tachibana, K. *J. Org. Chem.* **1999**, *64*, 866−876.
(26) Blin, K.; Medema, M. H.; Kazempour, D.; Fischbach, M. A.; Breitling, R.; Takano, E.; Weber, T. *Nucleic Acids Res.* **2013**, *41*, W204−12.
(27) Altschul, S. F.; Gish, W.; Miller, W.; Myers, E. W.; Lipman, D. J. *J. Mol. Biol.* **1990**, *215*, 403−10.
(28) Kim, B. C.; Lee, J. M.; Ahn, J. S.; Kim, B. S. *J. Microbiol. Biotechnol.* **2007**, *17*, 830−839.
(29) Chen, Y.; Wendt-Pienkowski, E.; Ju, J.; Lin, S.; Rajski, S. R.; Shen, B. *J. Biol. Chem.* **2010**, *285*, 38853−60.
(30) Duitman, E. H.; Hamoen, L. W.; Rembold, M.; Venema, G.; Seitz, H.; Saenger, W.; Bernhard, F.; Reinhardt, R.; Schmidt, M.; Ullrich, C.; Stein, T.; Leenders, F.; Vater, J. *Proc. Natl. Acad. Sci. U. S. A.* **1999**, *96*, 13294−9.
(31) Maruyama, C.; Toyoda, J.; Kato, Y.; Izumikawa, M.; Takagi, M.; Shin-ya, K.; Katano, H.; Utagawa, T.; Hamano, Y. *Nat. Chem. Biol.* **2012**, *8*, 791−7.
(32) Buntin, K.; Weissman, K. J.; Müller, R. *ChemBioChem* **2010**, *11*, 1137−46.
(33) Zhang, J.; Zhang, W.; Zou, D.; Chen, G.; Wan, T.; Zhang, M.; Cao, X. *Biochem. Biophys. Res. Commun.* **2002**, *297*, 1033−1042.
(34) Daubner, S. C.; Gadda, G.; Valley, M. P.; Fitzpatrick, P. F. *Proc. Natl. Acad. Sci. U. S. A.* **2002**, *99*, 2702−2707.
(35) Lei, B.; Shiao-Chun, T. U. *J. Bacteriol.* **1996**, *178*, 5699−5705.
(36) Ghisla, S.; Thorpe, C. *Eur. J. Biochem.* **2004**, *271*, 494−508.
(37) Gaitatzis, N.; Kunze, B.; Müller, R. *Proc. Natl. Acad. Sci. U. S. A.* **2001**, *98*, 11136−11141.
(38) Du, L.; Lou, L. *Nat. Prod. Rep.* **2010**, *27*, 255−78.
(39) Arastu-Kapur, S.; Anderl, J. L.; Kraus, M.; Parlati, F.; Shenk, K. D.; Lee, S. J.; Muchamuel, T.; Bennett, M. K.; Driessen, C.; Ball, A. J.; Kirk, C. J. *Clin. Cancer Res.* **2011**, *17*, 2734−43.
(40) Wang, Z.; Yang, J.; Kirk, C.; Fang, Y.; Alsina, M.; Badros, A.; Papadopoulos, K.; Wong, A.; Woo, T.; Bomba, D.; Li, J.; Infante, J. R. *Drug Metab. Dispos.* **2013**, *41*, 230−237.
(41) Fujii, K.; Ikai, Y.; Oka, H.; Suzuki, M.; Harada, K. *Anal. Chem.* **1997**, *69*, 5146−5151.
(42) Punta, M.; Coggill, P. C.; Eberhardt, R. Y.; Mistry, J.; Tate, J.; Boursnell, C.; Pang, N.; Forslund, K.; Ceric, G.; Clements, J.; Heger, A.; Holm, L.; Sonnhammer, E. L. L.; Eddy, S. R.; Bateman, A.; Finn, R. D. *Nucleic Acids Res.* **2012**, *40*, D290−301.
(43) Röttig, M.; Medema, M. H.; Blin, K.; Weber, T.; Rausch, C.; Kohlbacher, O. *Nucleic Acids Res.* **2011**, *39*, W362−7.
(44) Bachmann, B. O.; Ravel, J. *Methods Enzymol.* **2009**, *458*, 181−217.
(45) Ziemert, N.; Podell, S.; Penn, K.; Badger, J. H.; Allen, E.; Jensen, P. R. *PLoS One* **2012**, *7*, e34064.
(46) Baltz, T.; Baltz, D.; Giroud, C.; Crockett, J. *EMBO J.* **1985**, *4*, 1273−7.
(47) Räz, B.; Iten, M.; Grether-Bühler, Y.; Kaminsky, R.; Brun, R. *Acta Trop.* **1997**, *68*, 139−47.
(48) Huber, W.; Koella, J. C. *Acta Trop.* **1993**, *55*, 257−61.
(49) Cunningham, I. *J. Protozool.* **1977**, *24*, 325−9.
(50) Mikus, J.; Steverding, D. *Parasitol. Int.* **2000**, *48*, 265−9.
(51) Yang, M.; Arai, C.; Bakar Md, A.; Lu, J.; Ge, J.-F.; Pudhom, K.; Takasu, K.; Kasai, K.; Kaiser, M.; Brun, R.; Yardley, V.; Itoh, I.; Ihara, M. *J. Med. Chem.* **2010**, *53*, 368−73.
(52) Desjardins, R. E.; Canfield, C. J.; Haynes, J. D.; Chulay, J. D. *Antimicrob. Agents Chemother.* **1979**, *16*, 710−8.
(53) Matile, H.; Pink, J. R. L. In *Immunological Methods*; Lefkovits, I., Pernis, B., Eds.; Academic Press, San Diego, CA,1990; pp 221−234.
(54) Ponnudurai, T.; Leeuwenberg, A. D.; Meuwissen, J. H. *Trop. Geogr. Med.* **1981**, *33*, 50−4.
(55) Page, B.; Page, M.; Noel, C. *Int. J. Oncol.* **1993**, *3*, 473−6.
(56) Ahmed, S. A.; Gogal, R. M.; Walsh, J. E. *J. Immunol. Methods* **1994**, *170*, 211−24.
(57) Mosmann, T. *J. Immunol. Methods* **1983**, *65*, 55−63.
(58) Rachid, S.; Huo, L.; Herrmann, J.; Stadler, M.; Köpcke, B.; Bitzer, J.; Müller, R. *ChemBioChem* **2011**, *12*, 922−31.
(59) Groll, M.; Huber, R. *Methods Enzymol.* **2005**, *398*, 329−336.
(60) Kabsch, W. *Acta Crystallogr., Sect. D: Biol. Crystallogr.* **2010**, *66*, 125−132.
(61) Potterton, E.; Briggs, P.; Turkenburg, M.; Dodson, E. *Acta Crystallogr., Sect. D: Biol. Crystallogr.* **2003**, *59*, 1131−1137.
(62) Turk, D. *Acta Crystallogr., Sect. D: Biol. Crystallogr.* **2013**, *69*, 1342−1357.

DOI: 10.1021/jacs.5b03833
J. Am. Chem. Soc. 2015, 137, 8121−8130